Next Nanotechnology 7 (2025) 100111

Contents lists available at ScienceDirect

Next Nanotechnology

journal homepage: www.sciencedirect.com/journal/next-nanotechnology

Research article

Structural and morphological studies of non-covalent functionalization carbon nanotubes wrapped poly (3-hexylthiophene-2,5-diyl) nanocomposites

N. Abdullah [a,*], N.M. Nurazzi [b], I.P. Silverwood [c,d], S.K. Matam [d,e], S.Z.N. Demon [a], N.S.N. Sa'aya [a], N.A. Halim [a], K.W. Baharin [a]

[a] Centre for Defence Foundation Studies, National Defence University of Malaysia, Kem Sungai Besi, Kuala Lumpur 57000, Malaysia
[b] Bioresource Technology Division, School of Industrial Technology, Universiti Sains Malaysia, Penang 11800, Malaysia
[c] ISIS Pulsed Neutron and Muon Facility, Science and Technology Facilities Council, Rutherford Appleton Laboratory, Didcot OX11 0QX, UK
[d] UK Catalysis Hub, Research Complex at Harwell, Science and Technology Facilities Council, Rutherford Appleton Laboratory, Didcot OX11 0FA, UK
[e] Cardiff Catalysis Institute, School of Chemistry, Cardiff University, Cardiff CF10 3AT, UK

ARTICLE INFO

Keywords:
Inelastic neutron scattering
MWCNT
Non-covalent functionalization
P3HT
Structural
Sensor

ABSTRACT

In this study, a simple and efficient non-covalent functionalization method was developed to introduce conducting polymer of P3HT onto pristine MWCNT and hydroxyl MWCNT surfaces without causing significant changes in electrical characteristics, especially if used as a sensing material. Electron microscopy (FE-SEM) and (HR-TEM) were used to examine the surface morphology of nanocomposites, which demonstrated that the MWCNTs were well wrapped by P3HT. EDX analysis showed interactions between MWCNT-OH and P3HT, with a higher sulfur content of 7.77 wt% from P3HT. Additionally, the diameters of both pristine MWCNT (24.46 nm) and MWCNT-OH (27.56 nm) increased significantly when they form nanocomposites (35.35 nm and 39.40 nm respectively). Further characterization of the produced P3HT-MWCNT nanocomposite was performed using FT-IR and Raman spectroscopy. It was discovered that MWCNTs were dispersed uniformly, with a substantial interaction between P3HT and MWCNTs. The introduction of malathion on the surface of the nanocomposites reveals interaction between P3HT and malathion via intermolecular hydrogen bonding of thiophene, as evidenced by inelastic neutron scattering (INS) spectroscopy, suggesting that the P3HT/MWCNT has the potential as a promising sensing material for organophosphate compounds detection.

1. Introduction

Organophosphates (OP) compounds are chemicals formed as a result of the esterification process between phosphoric acid and alcohols. OP compounds are one of the most widely used pesticides in the agricultural industry worldwide [1]. The use of pesticides increases food productivity, but the residual presence of pesticides in food, water and the environment is a potential threat to human health and causes serious food contamination that severely affects ecosystems [2]. OP such as malathion [3], paraoxon [4], parathion [5], diazon and dichlorvos [6] are the most widely used in modern agriculture. OP compounds have been developed as warfare nerve agents such as tabun, soman, sarin, VX, and others [7]. This type of chemical warfare and their chemically-related pesticides both act as inhibitors of acetylcholinesterase (AChE). The main mechanism of the toxic OP can affect the nervous system and the respiratory system and lead to death [8]. Therefore, a sensitive and rapid detection method is urgently needed to monitor and detect harmful pesticides. The development of efficient selective sensors capable of detecting trace (ppm or sub-ppm) nerve agents in water and gaseous conditions is a major goal today to preventing the lethal consequences of terrorist attacks involving chemical weapons (CWA) [9,10].

Carbon nanotubes (CNTs) as sensing materials has garnered attention to fulfil the requirement as OP detector's. CNTs possess intriguing attributes such as a high surface-to-volume ratio and chemical stability, rendering them effective as highly sensitive chemical and biological sensors owing to their distinct electrical properties. These CNT-based sensors exhibit notable sensitivity, rapid response times, and room

* Corresponding author.
E-mail address: norli.abdullah@upnm.edu.my (N. Abdullah).

https://doi.org/10.1016/j.nxnano.2024.100111
Received 12 September 2024; Received in revised form 29 September 2024; Accepted 30 September 2024
Available online 3 October 2024

temperature operation [11,12]. However, despite their simplicity in fabrication and operation at ambient conditions, CNT-based sensors oppose challenges such as low responsiveness and relatively slow response durations [13]. Consequently, modifying the sidewalls of CNTs is proposed to enhance their dispersibility or solubility in solvents or polymers, thereby enhancing their interaction and reactivity with polymers through hydrogen bonding interactions. Moreover, surface modifications of nanotubes significantly impact their solubility characteristics, potentially influencing the ease of fabricating of CNT sensors. Hence, chemical modification of CNT sidewalls is necessary to enhance their dispersibility or solubility in solvents or polymers and to optimize interaction and reactivity with polymers via hydrogen bonding [14–16]. Furthermore, surface modification of nanotubes significantly influences their solubility characteristics, potentially impacting the fabrication process of CNT sensors[17,18].

Functionalization of carbon nanotubes (CNTs) is a widely used strategy to enhance their dispersion in organic media. Various methods are employed for the functionalization of CNTs, involving both covalent and noncovalent chemical reactions with a range of organic molecules, including polymers such as poly(3-hexylthiophene-2,5-diyl) (P3HT) [19], polyaniline (PANI) [20] or polypyrrole (PPY) [21]. Covalent functionalization typically involves creating stable chemical bonds between the CNT surface and functional groups, which improves solubility and compatibility with other materials.

The detection of malathion pesticide, using composites of polyaniline (PANI) and single-walled carbon nanotubes (SWCNTs) modified graphite electrodes has demonstrated high accuracy in malathion reduction [22]. Similarly, Linghao He [23] utilized PANI for the rapid determination of malathion, where uniformly distributed hollow carbon spheres (HCS) were wrapped with needle-like PANI nanowires, forming the HCS@PANI nanocomposite. This composite exhibited a high specific surface area, chemical functionality, and strong electrochemical activity. Additionally, Navpreet Kaur [24] developed a poly-3, 4-ethylenedioxythiophene (PEDOT) and carboxylated multi-walled carbon nanotubes (MWCNTs) based aptasensor for malathion detection, which was found to be highly specific and capable of detecting very low concentrations of malathion.

However, covalent functionalization can disrupt the intrinsic electrical and mechanical properties of carbon nanotubes. In contrast, noncovalent functionalization with conducting polymers enhances CNT-based materials without compromising their structure [25]. This method employs π-π stacking, van der Waals forces, and electrostatic interactions to attach conductive polymers to the CNT surfaces, preserving their exceptional electrical conductivity and mechanical strength while improving solubility and processability. The resulting composites exhibit synergistic properties, such as enhanced electrical performance and increased active surface area, making them ideal for applications in sensors[26], energy storage devices [27], and flexible electronics [28].

As discussed by Zhao et.al, [29]electrochemical properties of nanocomposites can be modified via non-covalent functionalization with small molecules, grafting or polymer wrapped nanotubes. The π-conjugated polymers serve as effective coatings for carbon nanotubes (CNTs) due to their enthalpic π-π interactions, ensuring stable dispersion. They can also be modified with synthetic receptors to enhance selectivity. SWCNTs-OH/PANI nanofibre composites with various thicknesses were synthesized via a simple in-situ chemical oxidative polymerization of aniline monomers on SWCNTs-OH for the detection of NH_3. The NH_3 gas sensing properties of the sensors were investigated and results showed that SWCNTs-OH/PANI composites exhibit enhanced NH_3 sensitive properties compared with the pure PANI [30]

Among all conductive polymers, poly(3-hexylthiophene-2,5-diyl) (P3HT), show fewer studied by researchers. P3HT, is a π-conjugated polymer, offers advantages such as cost-effective synthesis, remarkable environmental and thermal stability, mechanical strength, as well as magnetic and optical properties. It finds applications across a broad spectrum of usages [31]. P3HT disperse CNTs with specific chiralities and can isolate semiconducting SWCNTs and MWCNTs, resulting in P3HT/CNT nanocomposites with excellent oxidative stability. As per Munzer et al.,[32] regioregular polythiophenes (rr-P3HT) exhibit air-stable conductivity, making them well-suited for use as chemiresistive sensing materials. The polymer's backbone consists of interconnected thiophene rings, with the option to attach a chemical side-chain group to each ring and add an end-group or secondary copolymer chain to each end of the P3HT chain. Mahakul et al. [33] prepared MWCNT-incorporated rGO/P3HT ternary nanocomposites. Structural and morphological investigations revealed changes in the crystalline size and conjugation length of the polymer units, which are responsible for tailoring the optical, electrical, and electrochemical properties of the composites. The observed shift in the redox potentials after incorporating MWCNTs and rGOs into the P3HT host matrix is attributed to π–π interactions. The improvement in electrical properties of the composites is due to the softening of the interfacial grain boundary by the 3D network structure created by the well-dispersed MWCNTs and rGOs in the P3HT matrix.

Chemiresistive sensors, which operate by measuring changes in conductivity, have found widespread applications in various fields. The incorporation of carbon nanotubes (CNTs) and polymer composites has significantly enhanced the performance of these sensors. Kim et al. [34] recently reported a novel composite material comprised of CNTs and covalently functionalized poly(3-hexylthiophene) (TFMK-P3HT). This new composite demonstrated a remarkable four-fold increase in sensitivity to amines compared to previously developed materials. Notably, the sensor exhibited high selectivity, stability in humid environments, and was unaffected by other gases. Neuroscience research has also benefited from the utilization of P3HT-MWCNT composites. Meng Z et al. [35] successfully employed these materials to monitor neurochemical processes, shedding light on glutamate-induced brain edema and the release of ascorbic acid. A P3HT/N-MWCNT composite microelectrode was strategically introduced for the detection of ascorbic acid, showcasing exceptional selectivity, stability, and biocompatibility.

Several techniques are gaining interests for characterizing the molecular structure of nanocomposite materials. Among these, Fourier transform infrared (FTIR), Raman, and inelastic neutron scattering (INS) spectroscopies play pivotal roles and complement each other. Raman spectroscopy detects the relative frequencies at which a sample scatters radiation, relying on changes in molecular polarizability. Conversely, IR spectroscopy measures the absolute frequencies at which a sample absorbs radiation, depending on changes in dipole moment. INS spectroscopy, however, is not bound by these selection rules. In terms of molecular sensitivity, Raman spectroscopy excels in detecting homonuclear molecular bonds such as C-C, C═C, and C≡C, while FTIR spectroscopy is adept at detecting hetero-nuclear functional group vibrations and polar bonds like hydroxyl (OH), carbonyl (CO), and amide bonds [36,37].

INS has been employed to deduce diverse material properties, encompassing the local structure of polymers, binding interactions within porous materials, and protein folding dynamics [38,39]. It offers a distinctive insight into the structural dynamics of hydrogenous materials, a perspective often inaccessible to optical techniques like FTIR and Raman spectroscopy. Notably, INS exhibits signal strength proportional to nuclear displacement and cross section, rendering it highly sensitive to hydrogen. Its lack of selection rules makes it particularly well-suited for the current study [40]. Furthermore, INS provides comprehensive coverage of the entire molecular vibrational range, including the low-frequency region of the vibrational spectrum [41]. Therefore, INS can enhance the fundamental understanding of interactions between individual components in nanocomposites, crucial for establishing the connection between composite structure and properties. By confirming the formation of nanocomposite materials rather than mere mixtures of independent components, INS provides insights that can be leveraged to optimize and tailor the properties of these materials. This, in turn, enables the overcoming of scientific and

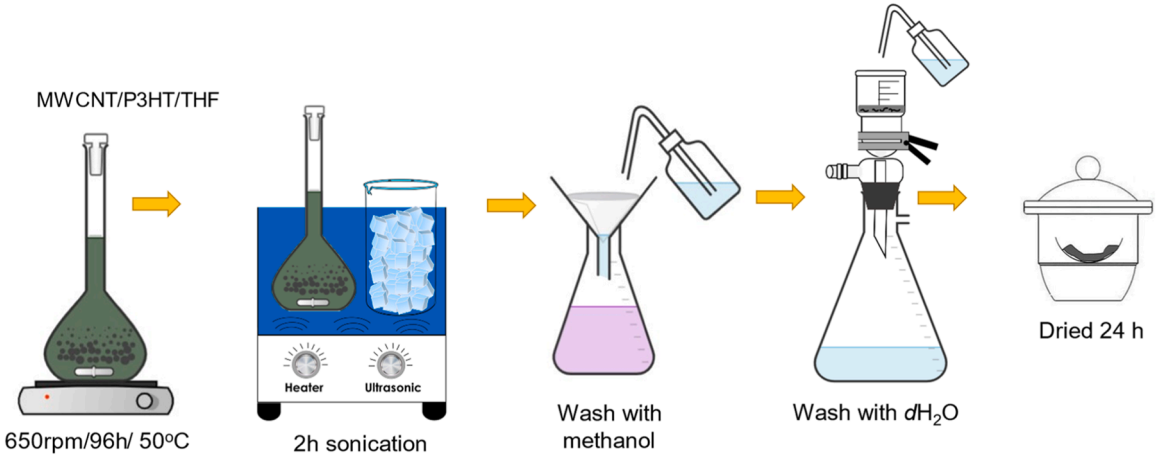

Fig. 1. Schematic diagram for preparation of P3HT wrapped carbon nanotubes.

technological challenges inherent in their production.

In this present work, we focus on characterizing the structural and morphological properties of non-functionalized multi-walled carbon nanotubes (MWCNTs) incorporated into P3HT host systems. Less work has been conducted on the interaction between pristine and functionalized MWCNTs and polymers. It is known that surface morphology plays an important role in selecting suitable candidates for sensing materials. Therefore, our experimental approach centers on examining the structural and morphological alterations in the composite system following the introduction of malathion, employing a combination of FTIR, Raman, INS, FESEM, and HRTEM techniques. Notably, we present, to the best of our knowledge, the first application of the INS technique to elucidate the interaction between P3HT, MWCNT-OH, and malathion.

2. Experimental

2.1. Materials

Pristine multiwalled carbon nanotubes (MWCNT) (purity >95 %) and hydroxyl-functionalized multiwalled carbon nanotubes (MWCNT-OH) (purity >95 %) were purchased from Nanostructured & Amorphous Materials. Poly(3-hexylthiophene-2,5-diyl) regioregular P3HT (P), with a Mw ranging from 50,000 to 100,000 with a purity of ~90 % was obtained from Sigma-Aldrich. Tetrahydrofuran (THF) organic solvent and methanol (CH_3OH) were also purchased from Sigma–Aldrich and R&M Chemicals respectively. All materials and solvents were used as received without further purification.

2.2. Nanocomposites preparation

The procedure for preparing nanocomposites was adopted from our previous work [42,43] and depicted in Fig. 1. Initially, 15 mg of pristine multiwalled carbon nanotubes and 15 mg poly(3-hexylthiophene-2,5-diyl) were mixed in a 50 mL volumetric flask. Subsequently, 15 mL of THF was added to the flask. The flask was placed on a heating plate and the suspension was stirred continuously at 650 rpm for 96 hours at 50°C. Following this, the flask was transferred and underwent sonication in a water bath operating at a frequency of 50 Hz for 2 hours, maintaining a controlled temperature between 25°C and 30°C using ice cubes. The resulting nanocomposite, displaying a dark olive green color, was washed repeatedly with methanol solution until the mixture became colorless. Subsequently, it was washed with deionized water and filtered using a vacuum buchner funnel with nylon membrane filters (47 mm diameter, 0.2 μm thickness). The obtained black powder was dried at room temperature for 24 hours. The yield of nanocomposites from these experiments was consistently high, ranging from 90 % to 95 %. To explore the effect of functionalization, the same procedure was repeated with hydroxyl-functionalized multiwalled carbon nanotubes using identical quantities of materials and chemicals.

Table 1
Composition and sample coding of the nanocomposites.

Sample code	Composition	Functional group
NT-P	MWCNT + P3HT	-
NT-OH-P	MWCNT-OH + P3HT	OH
NT-P-malathion	MWCNT + P3HT + malathion	-
NT-OH-P-malathion	MWCNT-OH + P3HT+malathion	OH

2.3. Nanocomposites/malathion preparation

2.0 mg of pristine MWCNT and MWCNT-OH, as well as the fabricated MWCNT/P and MWCNT-OH/P nanocomposites, were each combined with 60 μL of malathion (0.1 M). The nanocomposites treated with malathion were designated as NT-P-M and NT-OH-P-M, respectively. Table 1 provides a comprehensive list of sample codes and their corresponding nanocomposites.

3. Characterization

3.1. Raman spectroscopy

The Raman spectroscopy analysis was carried out using Renishaw in Via Reflex Confocal Micro Raman System (Renishaw plc, Wotton-under-Edge, UK) calibrated using silicon at peak of 520 nm. The Raman spectra was taken at room temperature and sample excitation was set at a wavelength of 787 nm, 1200 mm^{-1} gratings, 1.00 s^{-1} exposure time, 5 % laser power with accumulations of 1. The magnification was focused by a 100× objective lens.

3.2. Fourier transform infrared spectroscopy (FTIR) analysis

FTIR spectra were collected on a Perkin Elmer Frontier spectrometer FTIR within the 500–4000 cm^{-1} scanning range by accumulating 16 scan numbers, with spectral resolution of 4 cm^{-1}, DTGS detector was used for the measurement. Each sample was mixed with potassium bromide (KBr) at a 1:9 ratio to obtain better signal.

3.3. Scanning electron microscopy (SEM) and Energy dispersive X-ray (EDX) analyses

The surface morphological analysis on the effectiveness of P3HT

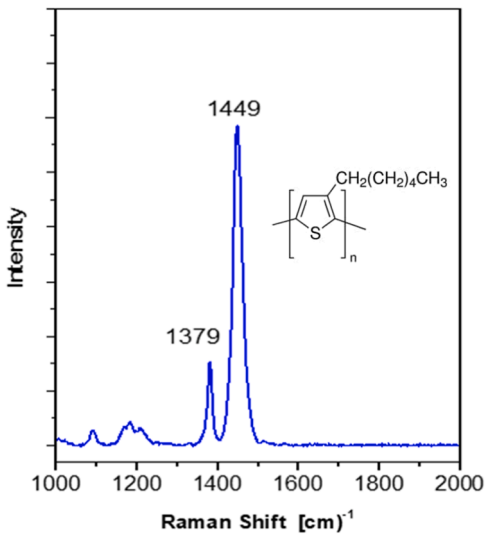

Fig. 2. Raman spectra of pristine P3HT.

wrapping onto MWCNT and after exposure with malathion was characterised using a Field Emission Scanning Electron Microscopic (FESEM), Carl Zeiss Gemini FESEM 500 (Carl Zeiss AG, Jena, Germany). Prior to the analysis, samples were initially coated with gold for about 1 min in order to avoid charging.

3.4. Transmission electron microscope (HRTEM)

Further analysis on the morphological of nanocomposites was observed under a High-Resolution Transmission Electron Microscope (HRTEM), JEOL JEM 2100 F HRTEM (Tokyo, Japan) at an acceleration voltage of 200 kV. For HRTEM analysis, the sample was initially dispersed in acetone by ultra-sonication for 60 s. Subsequently, a drop of the suspension was transferred onto a carbon-coated copper grid and mounted on the microscope, and the images were recorded.

3.5. Inelastic neutron scattering (INS)

INS data was recorded using the TOSCA spectrometer at the ISIS neutron and muon source in the UK. Samples were loaded into indium-sealed aluminium sample holders and loaded into the instrument and cooled using closed cycle refrigerators. Data were collected at temperatures below 30 K.

4. Results and discussion

4.1. Raman spectra

Raman spectroscopy is extensively employed in the analysis of MWCNTs due to its capability to provide insights into the degree of structural disorder and the interaction of P3HT and MWCNTs. The Raman spectra of pristine P3HT is shown in Fig. 2, while pristine MWCNTs Functionalized MWCNTs together with their nanocomposites are compared in Fig. 3. The pristine P3HT show two main in-planes thiophene ring modes of C=C symmetric stretching at 1449 cm^{-1} and peak around 1379 cm^{-1} associated with the C-C stretching mode of the thiophene ring [44,45].

Whereas, for pristine MWCNTs (Fig. 3a), three dominating features are seen. Two sharp Raman peaks, namely G (graphite), D (disorder) bands are seen together with their second-order harmonic (the G' band). The D band, observed at 1312 cm^{-1}, represent a represents a double-resonance Raman mode, indicative of a disordered structure or lattice defects within the graphite lattice (such as substitutional heteroatoms, vacancies, or chemically bonded heteroatoms). In contrast, the peak at 1605 cm^{-1} corresponds to the G band, signifying a carbon vibration in the circumferential direction. This band represents the high-frequency $E_{2\,g}$ first-order mode of a well-ordered graphitic structure [46,47]. The Raman spectrum of pristine also exhibits a band at 2611 cm^{-1} called the G' band. This second-order overtone of the D-band is related to the two-phonon scattering process and provides information about the number of layers and stacking order in MWCNTs. Apparently, for functionalized MWCNTs (Fig. 3b) all three of this band slightly shifted to a lower wavenumber (1290, 1580 and 2588 cm^{-1}). The shift of the G′

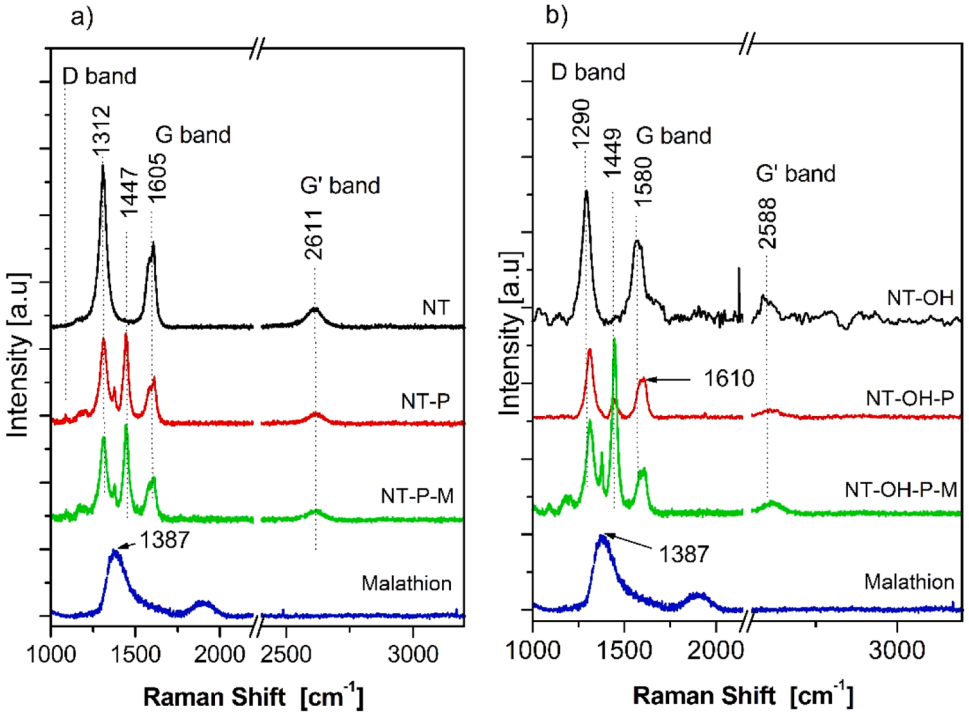

Fig. 3. Raman spectra of pristine MWCNTs (a) and functionalized MWCNTS (b).

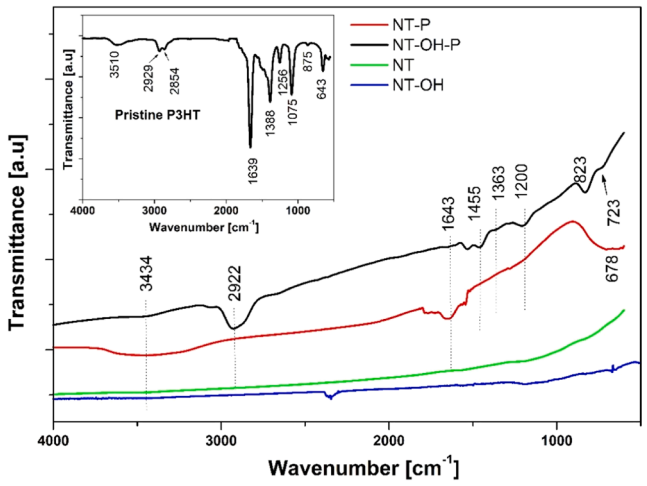

Fig. 4. FTIR spectra of P3HT (inset) and CNT nanocomposites.

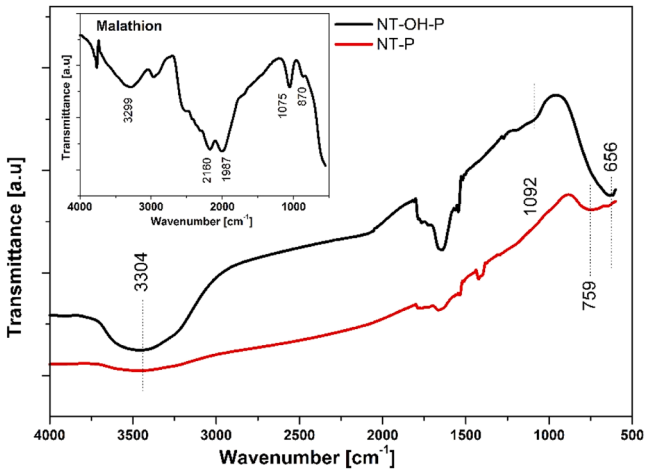

Fig. 5. FTIR spectrum of malathion (inset) and CNT nanocomposites after exposure to malathion.

peak to a lower wavenumber is often a sign that the functionalization has altered the structural and electronic properties of the carbon nanotubes as in this case hydroxyl group that attached to the outer-walled of carbon nanotubes. In addition, shift of g' band to 2588 cm^{-1} suggest that the G' band attributable to the overtone of the D band indicative of electron transfer from CNT to OH species on the surface[48].

Compared with pure P3HT and the nanocomposites, the incorporation of NT and NT-OH into P3HT matrix has revealed the slight red shift of the D-band and G-band in the nanocomposite and with an additional peak from thiophene appearing at 1447 cm^{-1}. The slight red shift of these bands suggesting the ground state interaction and appreciable charge transfer between nanotubes and the polymer. This phenomenon can be attributed to the increase in the conjugation length of the polymer chain and increased conjugation length of the grafted P3HT, which might be due to the crowding of the P3HT chains grafted on nanotubes walls [49,50]. Furthermore, the peak around 1379 cm^{-1}, corresponding to the C-C stretching mode of the thiophene ring of P3HT, is not visible in the Raman spectra of the nanocomposites because it is obscured by the peaks of CNTs [51]. A similar observation was reported by Maity et al. (50) for PANI/MWCNT composites [52]. NT-OH-P nanocomposites show up shift of G band at 1610 cm^{-1} and slightly shift of G' band in NT-OH (2593 cm^{-1}) to NT-OH-P (2588 cm^{-1}). This indicating substantial charge transfer interactions between NT-OH and P3HT [53,54]. Raman spectra for NT and their nanocomposites (Fig. 3b) show similar behavior to NT-OH for the D band and the G band. Whereas the G' band are at the same position after the introduction of P3HT wrapping. This signifies no substantial charge transfer interaction between NT and P3HT. This is probably due to the absence of surface oxygen functional group (SOFG) on the CNT surface. According to Michele et. al [55], this shifted up can be attributed to two primary causes: nanotube doping and mechanical restriction of C–C vibration freedom. In terms of doping, an up-shift in the G band may occur if carbon nanotubes donate electrons to the interacting material. On the contrary, the restriction of C–C vibrations can be attributed to non-covalent interactions between nanotubes and polymers, such as π–π or CH–π interactions.

The ratio between the intensities of the G and D bands is a quantitative indication of the amount of functional groups introduced, by measuring the sp3 carbon atoms. As the lower the ratio, the higher the amount of sp3 carbon atoms; in other words, higher the amount of functional groups. The I_D/I_G ratio obtained for Raman spectra of non-covalent functionalization of NT-OH-P (1.8) is higher than the pristine NT-OH (1.6), indicating disordered structures/defects are created after introduction of P3HT [56,57]. While that of pristine NT-P (1.91) is similar to pristine NT (1.94) implying that the structure of nanocomposites was maintained after functionalization without introducing structural defects. When a droplet of malathion aqueous solution with 60 μL in volume was introduced onto the NT-P and NT-OH-P nanocomposites, the main characteristic bands of malathion molecule at 1387 cm^{-1} can be seen whereas the band at 1880 cm^{-1} disappears [58]. The increased intensity of this vibration peak of malathion in the NT-OH nanocomposite sample, compared to the sample without the OH functional group, can be attributed to intermolecular forces through hydrogen bonding interactions. Conversely, pristine MWCNTs lack these hydrogen bonding interactions due to the absence of functional groups.

4.2. FTIR spectra

The FTIR spectra of P3HT and its nanocomposites are displayed in Fig. 4. The IR absorption bands of the thiophene ring are found between 500 and 2000 cm^{-1}. P3HT exhibits characteristic peaks at 2929, 2854, 1639, 1388, 1256, 1075, 875, and 643 cm^{-1}. The bands at 2929 cm^{-1} and 2854 cm^{-1} are assigned to the -CH_2 in-plane mode and the -CH_3 asymmetry mode, respectively. The peaks at 1639 and 1388 cm^{-1} are associated with the C═C asymmetric and symmetric stretching vibrations of the thiophene ring [59]. The band at 1256 cm^{-1} corresponds to C-C stretching vibrations, while the C–S stretching in the thiophene ring is observed at 1075 cm^{-1}. The band at 875 cm^{-1} is due to the out-of-plane C–H vibration of the 2,5-substituted thiophene monomer, and the peaks at 643 cm^{-1} are attributed to the C-S stretching in the thiophene ring[60]. It can also be observed that the vibrational frequencies present in P3HT are visible in the spectra of NT-P and NT-OH-P nanocomposites. For the NT-OH-P composites, the spectra show a mixture of characteristic absorption bands from both MWCNTs and P3HT. Some peaks attributed to P3HT are slightly shifted, such as the C-C vibration at 1200 cm^{-1}, the out-of-plane C–H vibration of the thiophene monomer at 823 cm^{-1}, and the C-S stretching in the thiophene ring at 723 cm^{-1}[61]. These shifts indicate an interaction between the MWCNTs and P3HT. The intensity of band responsible of P3HT groups decrease presumably cause by interaction of P3HT with OH functional group in NT-OH through hydrogen bonding interaction [62]. In the case of NT-P, the absence of band position shifts indicates that there are no strong interactions between P3HT and MWCNT, apart from π–π stacking, rather than interactions through hydrogen bonding formation. However, a new absorption peaks at 1455 cm^{-1} and 1643 cm^{-1} are present, suggesting atomic vibrations related to the P3HT wrapped on the nanotube walls for both nanocomposites, as observed in the SEM images. We can conclude that the slightly reduced peak intensities in all spectra indicate that polythiophene has successfully wrapped around the surface of the nanotubes.

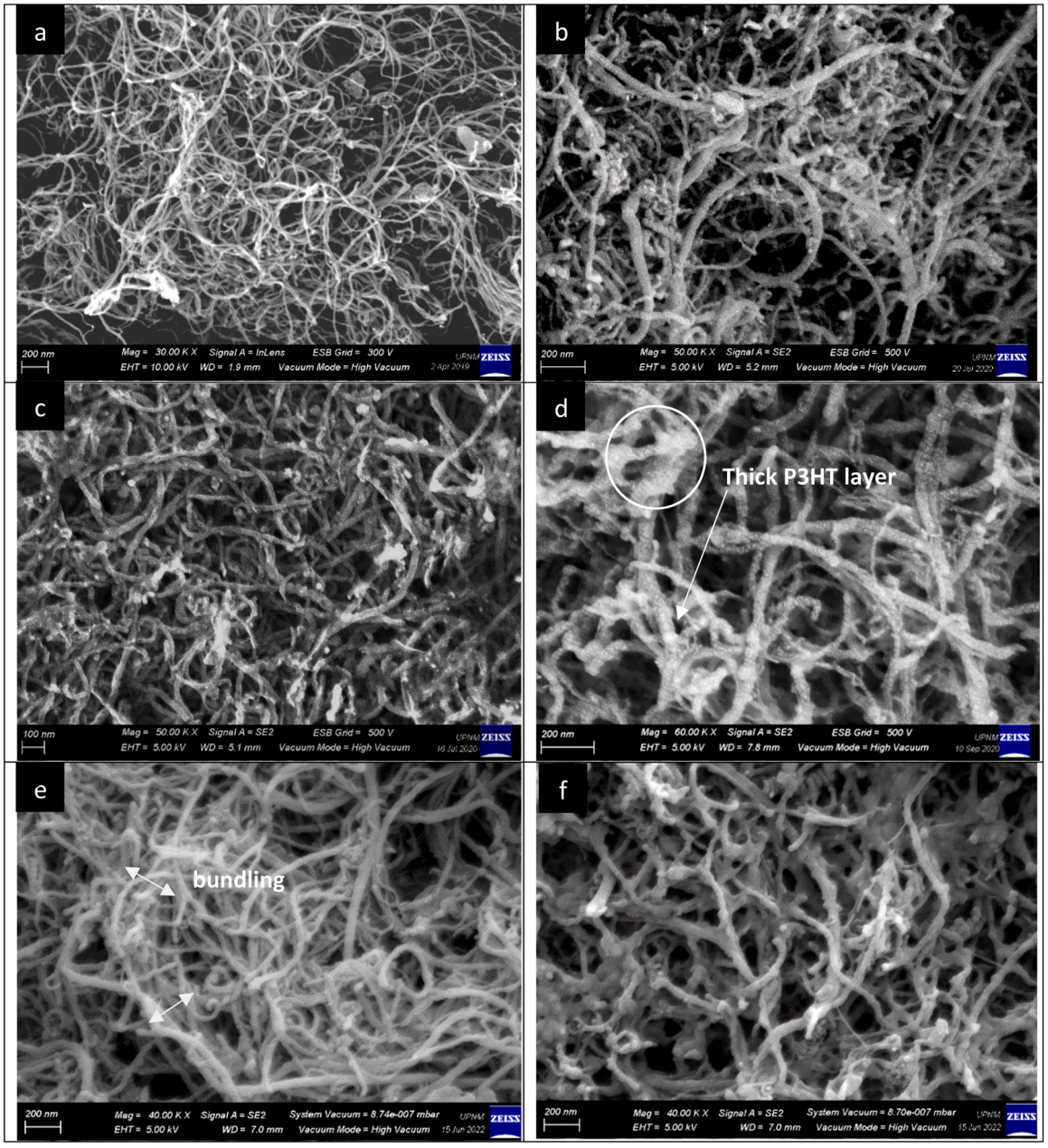

Fig. 6. FESEM images of pristine carbon nanotubes, NT (a), NT-OH (b), nanocomposites of (c) NT-P, (d) NT-OH-P, nanomposites after exposure to malathion (e) NT-P-M and (e) NT-OH-P-M.

FTIR spectra of nanocomposites after introduction of malathion are depicted in Fig. 5. Spectra of malathion (inset) shows a band at 1075 cm^{-1} corresponding to the stretching of P-OCH_3 group, the P-S bond was linked to ~870 cm^{-1} and C-S bond appear at ~620–715 cm^{-1}. The spectrum of NT-OH-P nanocomposite shows the characteristic behavior of the functional groups that are present in the adsorbed malathion molecule at 1092 cm^{-1} and 656 cm^{-1} [63]. Whereas for NT-P only band at 759 cm^{-1} appear which related to the characteristic of malathion. This suggest that the interaction of malathion molecule with the NT-OH nanocomposite occurs due to intermolecular interactions through hydrogen bonding. These results confirm with our Raman data (Section 4.1).

4.3. Morphology study

Field emission scanning electron Microscopy (FESEM) was employed to study the surface morphology of the multi-walled carbon nanotubes nanocomposites. The result (Fig. 6) of pristine MWCNT and hydroxyl functionalized MWCNT displayed some network-like, curved, random entangled structures that form three-dimensional networks. The overall surface of the tubes showed smooth surface texture. Particularly for pristine MWCNT, the sample has far more uniform tubes, curve but with uniform diameter distribution as seen in Fig. 6(a). In contrast, for NT-OH in Fig. 6(b), two kinds of tubes were observed in the sample; one was relatively thick MWCNT, the other appeared as grass-like agglomerates at certain area. From the images of nanocomposites, it can be seen the changes in their morphology after P3HT was successfully wrapped the outer wall of the MWCNTs. The diameter of the tubes of NT-P nanocomposites enlarge and the surface become slightly coarse with no concentrate P3HT agglomerate in the sample, meaning that P3HT covered each MWCNTs making a thin layer around the tubes as depicted in Fig. 6(c). For NT-OH-P in Fig. 6(d) highly saturated, thicker and

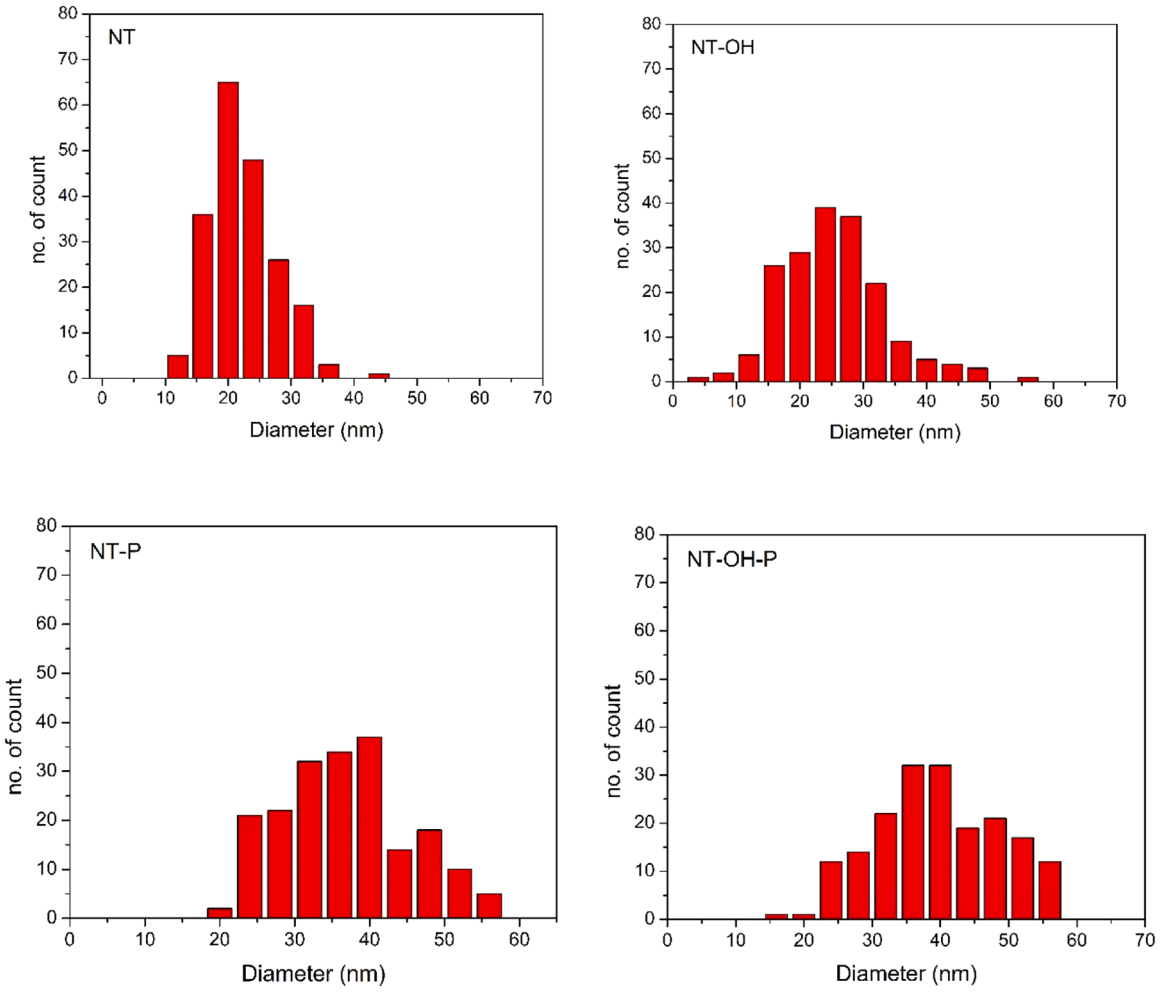

Fig. 7. Histogram of diameter size distribution of pristine NT, pristine NT-OH, NT-P nanocomposites and NT-OH-P nanocomposites.

unsmooth layer covering MWCNTs by P3HT were spotted in the sample. This might be due to OH functional group in NT-OH that is responsible for the hydrophilic properties. Fig. 6(e-f) displays FESEM images of NT-P and NT-OH-P nanocomposites after exposure to malathion molecules. Upon exposure, changes in the morphology of the nanocomposites, such as aggregation and bundling of CNTs, can be observed due to alterations in surface energy. Malathion molecules may introduce new intermolecular forces, such as van der Waals forces or hydrogen bonds, between the CNTs. These additional forces can draw the nanotubes closer together, resulting in bundling (Fig. 6(e)).

The average particles size distribution was determined by ImageJ software based on 200 data points in FESEM images. The histogram of the diameter variation is shown in Fig. 7. An average of diameter size together with their standard deviation (stdev) of the pristine CNTs are 24.46 nm (stdev ± 5.42) and 27.56 nm (stdev ± 8.2) for NT and NT-OH, respectively. For nanocomposites samples their diameter size are 35.35 nm (stdev ± 10.73) and 39.40 nm (stdev ± 9) for NT-P and NT-OH-P, respectively. This demonstrated that P3HT was successfully wrapped around the CNT tubes using a non-covalent functionalization process. This finding is consistent with our Raman and FTIR data, where peaks indicative of polymer wrapping are evident in each spectrum. Additionally, our work on MWCNT-OH nanocomposites prepared at different reaction times showed an increase in diameter. The longer the suspension of MWCNT in the P3HT matrix, the greater the diameter of the MWCNT-OH nanocomposites [42].

The nanocomposites samples were introduced with malathion and the excess was allowed to evaporate prior to further EDX analysis. EDX elemental mapping of carbon (C), oxygen (O) and sulfur (S) in Fig. 8 clearly reveals that the sulfur element is evenly distributed throughout CNT matrix. A similar finding by Madhusudhan et al. [64]demonstrated the incorporation of MWCNT and its interaction with polypyrrole, as evidenced by EDX analysis. Elemental composition of the NT-P composite obtained from EDX analysis indicated the presence of carbon, oxygen and sulfur as the major elemental components with the weight percentage of 93.18 %, 1.05 % and 5.78 %, respectively, over the entire region of the prepared sample. Whereas for NT-OH-P the weight percent are 90.84 %, 1.39 % and 7.77 %. This result confirms the presence of sulfur, which originates from the heterocyclic thiophene (P3HT) unit homogenously distributed on carbon nanotubes. The interaction of NT-OH wrapped with P3HT was stronger than NT without OH functional groups on the surface, as can be seen from the higher wt% of sulfur in NT-OH of 7.77 %. However, there is no trace of phosphorus related to malathion molecule on the samples indicating this target analyte weakly interacted with the nanocomposites.

This conclusion is also supported by our previous results, which involved electrical measurements of P3HT and P3HT/MWCNT-OH nanocomposite films using carbon electrodes. The incorporation of MWCNT-OH enhanced the charge transport properties of the P3HT nanocomposite, increasing the current to up to 8 mA [15]. In contrast, the amperometric measurement of P3HT/MWCNT-OH increased by 85 % compared to pristine MWCNT, indicating an improved charge carrier pathway in the MWCNT-OH composite upon malathion exposure. The change in current (ΔI) for P3HT/MWCNT-OH was significantly larger than that of the pristine MWCNT[65]. We also observed the

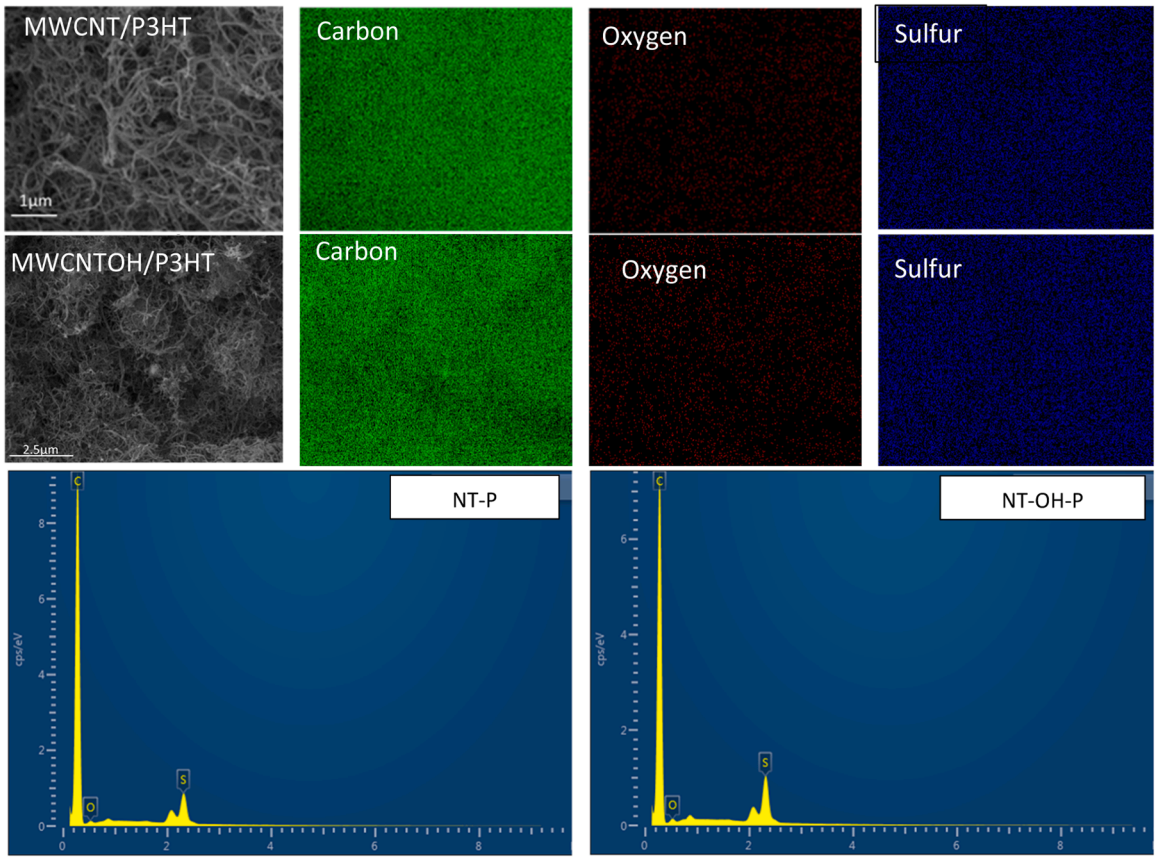

Fig. 8. EDX mapping of P3HT carbon nanotubes nanocomposites.

presence of hydrogen through Raman and FTIR data; however, it could not be detected by EDX due to its low Z contrast. The presence of hydrogen will be further discussed in the INS data presented in Section 4.4.

The morphology of the nanocomposites were further characterized by HRTEM. As can be seen in Fig. 9(a) and (b) for MWCNT and MWCNT-OH nanocomposites after exposure with malathion respectively. Both MWCNT samples is tubular in shape with thin layer of P3HT wrapped on the nanotubes walls. The thickness of the P3HT layer was found to be around 3 nm and the diameter of the nanotubes was found to be 10 nm. It was hard to observe the changes on the morphology and dispersion of NTs nanocomposite in P3HT matrix before and after their exposure with malathion.

4.4. *Inelastic neutron scattering*

Fig. 10 shows the spectra of the pristine and functionalized nanotubes. The OH functionalized MWCNT has greater intensity in a broad band around 620 cm^{-1}. The breadth of this feature suggest that OH moieties are present in a number of different environments due to variation in the hydrogen bonding network between surface OH species as the neutron scattering intensity (S) depends on the quantity of material in the beam as well as the neutron scattering cross section of the sample, these and subsequent spectra were normalized and offset for plotting. Many of the features at low energy are due to inter-molecular vibrations that are hard to assign without computational simulation.

The spectra for the MWCNT samples with P3HT are shown in Fig. 11 and are almost identical to each other and to the unbound P3HT. Two possibilities are immediately suggested. Firstly, it is possible that the recorded signal is dominated by bulk P3HT with a substantial excess of polymer causing the signal from the unbound polymer overwhelming that of the P3HT interacting with the MWCNT. The second possibility is that the P3HT is not strongly affected by binding to the nanotubes. It should also be remembered that as INS is most sensitive to scattering from hydrogen atoms, due to their large incoherent neutron scattering cross section, there is comparatively little contribution from the composite nanotube systems. Whereas, the NT-P malathion and NT-OH-P malathion spectra are displayed in Fig. 12, with the P3HT and malathion spectra for reference. The malathion spectrum is relatively noisy resulting from the low sample mass measured due to its hazardous nature. The nanotube systems show intense peaks at 425 and 580 cm^{-1}, which were not present in the P3HT samples without malathion (Fig. 11). Furthermore, the band structure between 700 and 900 cm^{-1} is simplified when malathion is present, showing only three bands compared to five in the P3HT, NT-P and NT-OH-P. The change in these bands is assigned to the distortion of the thiophene ring around the sulfur in the polymer [41,66]. Alternatively, the 425 cm^{-1} feature could is also in the range that may be expected from a longitudinal acoustic phonon mode [27,67] and the 580 cm^{-1} peak could represent a sharpening of the OH feature present on the NT-OH sample. Since it is also present in the non-functionalized materials, the thiophene C-S-C stretch would seem the most likely interpretation when considered with the other spectral changes.

Fig. 13 shows the low energy region of the spectra from the P3HT coated samples with and without malathion. The samples show strong methyl torsions, with the NT-P and NT-OH-P showing a maximum at 244 cm^{-1}. The malathion containing samples have this shifted to non-OH functionalized peak to 258 cm^{-1} and to 260 cm^{-1} in the OH functionalized material. This further demonstrates a clear interaction between malathion and the polymer. These findings complement the EDX analysis and corroborate the Raman and FTIR data. In conclusion, the INS spectra shows that although the OH functionalization of the MWCNT is present it does not appear to have a strong effect on the spectra obtained with P3HT and malathion. However, there is strong

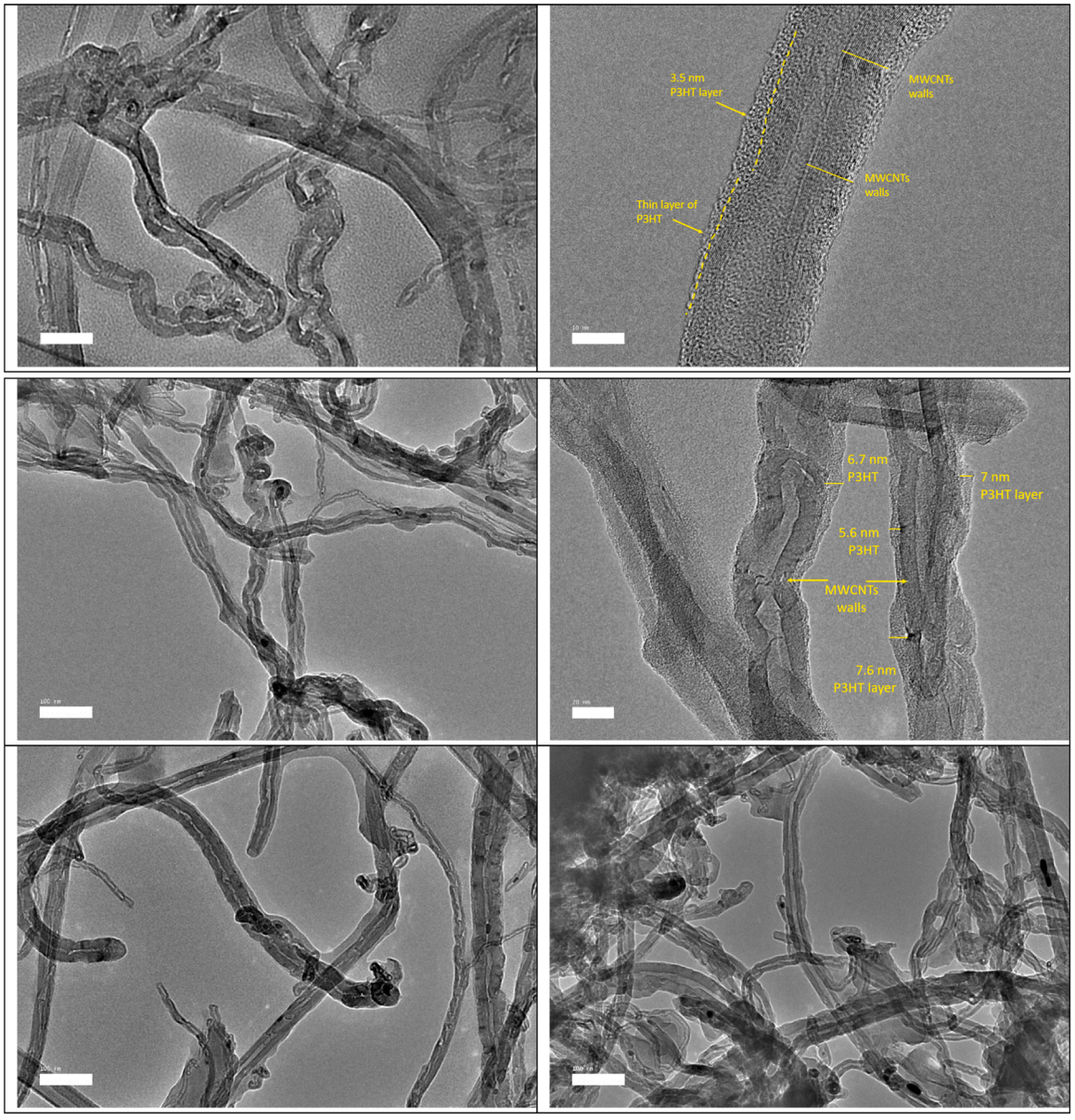

Fig. 9. HRTEM analysis of NT-P nanocomposites (a-b) NT-OH-P nanocomposites (c-d) and nanocomposites exposed to malathion NT-P-M (e) and NT-OH-P-M (f).

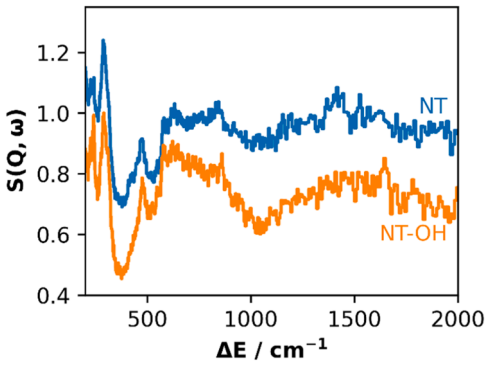

Fig. 10. Normalized INS spectra of unfunctionalized MWCNT (NT) and OH functionalized MWCNT (NT-OH) showing increased signal of the functionalized nanotubes centred at 620 cm-1. Spectra are offset for clarity.

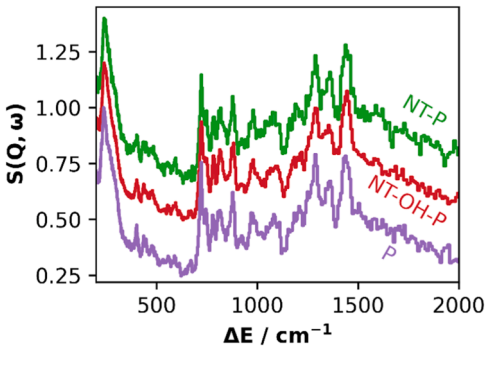

Fig. 11. INS spectra of pure P3HT (P), and its interaction with unfunctionalized MWCNT (NT-P) and OH functionalized MWCNT-P3HT (NT-OH-P) after normalization The spectra are almost identical and have been offset for clarity.

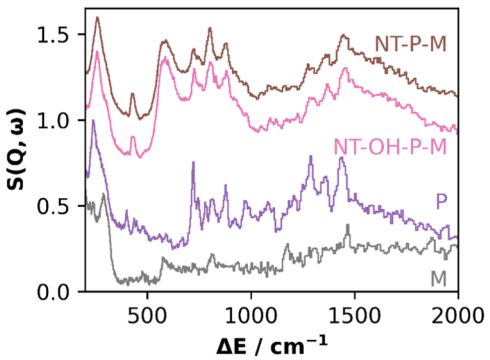

Fig. 12. Shows the spectra of the two nanocomposites (NT-P-M and NT-OH-P-M) samples interacting with both malathion and P3HT, alongside the pure P3HT (P) and malathion (M) for comparison. The weaker features in the malathion spectrum are due to the volume of the sample recorded. Only a very small quantity was measured due to its hazardous nature. The malathion shows peaks at 570, 810, 1155 and 1450 cm^{-1}.

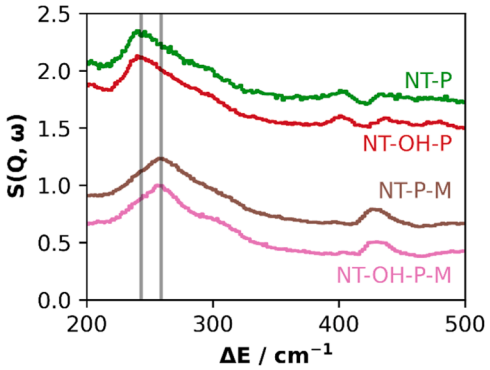

Fig. 13. Comparison of the normalized spectra obtained from P3HT coated MWCNT (NT-P) and MWCNT OH (NT-OH-P) and with malathion (NT-P-M and NT-OH-P-M respectively) at low energy transfer. Lines to indicate the shift of the methyl torsion are included at 244 and 259 cm^{-1}. Plots are offset for clarity.

evidence that the polymer interacts with malathion through the thiophene ring on the polymer chain.

4.5. Significance and limitation

The significance of this study lies in its development of a simple and effective method for non-covalently wrapping polythiophene (P3HT) onto pristine and hydroxyl-functionalized multi-walled carbon nanotubes (MWCNTs). The study demonstrates stronger interactions between P3HT and hydroxyl-functionalized MWCNTs, as evidenced by EDX analysis. Characterization techniques such as FTIR and Raman spectroscopy reveal significant interactions between the P3HT and MWCNTs, suggesting the potential for the formation of nanocomposites. The interaction between P3HT and malathion, observed through INS spectra, indicates the possibility of using these nanocomposites as sensors for organophosphate compounds. This research provides valuable insights into the synthesis and characterization of carbon-based conductive polymer materials, paving the way for future advancements in sensor technology.

However, the limitation about this study is the potential for non-covalent functionalization to result in weak interactions between P3HT and MWCNTs. This could compromise the long-term stability and durability of the nanocomposites, particularly in challenging environmental conditions. While electron microscopy and spectroscopy techniques offered valuable insights, they may not fully capture the nanoscale interactions and electrical properties at the atomic level. Additionally, the study primarily concentrated on surface-level interactions, and bulk properties were not extensively explored. Furthermore, the sensing performance was exclusively evaluated with malathion, restricting the generalizability of the findings to other organophosphate compounds. Future studies are necessary to assess the selectivity and long-term performance of these nanocomposites in detecting a broader range of analytes. By addressing these limitations, future research can contribute to the development of more robust and versatile nanocomposite-based sensors for environmental monitoring and other applications.

5. Conclusion

In summary, a simple and efficient non-covalent wrapped method to introduce P3HT onto the pristine MWCNT and MWCNT-OH surfaces has been successfully fabricated and characterized. The interaction of MWCNT-OH wrapped with P3HT was stronger than pristine MWCNT on the tube surface as observed from EDX analysis with the higher amount of sulfur from P3HT being about 7.77 wt%. Whilst, the diameter of pristine MWCNT increased from 24.46 nm to 35.35 nm and from 27.56 nm to 39.40 nm for MWCNT-OH, respectively. FTIR and Raman Spectra show systematic shifting in the position of characteristic bands and peaks of P3HT due to a significant interaction between the MWCNT-OH with the P3HT. The effect of deposited malathion on the nanocomposites has shown that intermolecular interactions occur between P3HT and malathion between thiophene group and sulfur from P3HT respectively as shown from INS spectra. From the INS results, the malathion spectrum is relatively noisy resulting from the low sample mass measured due to its hazardous nature. The nanotube systems were not present in the P3HT samples without malathion. Accordingly, the findings from this research are expected to provide an insight about the potential of MWCNT/polymer nanocomposites that it can be utilized as a sensor material for detection organophosphate compounds. Moreover, this new synthetic method can be easily applied to the synthesis of other carbon-based conductive polymer materials.

CRediT authorship contribution statement

N. Abdullah: Conceptualization, Data curation, Formal analysis, Funding acquisition, Writing – original draft. N. M. Nurazzi, N. S. N. Sa'ayaa: Methodology, Validation, Resources, Writing – review & editing. I. P. Silverwood, S. K. Matam: Data analysis, Formal analysis, Writing – review. S. Z. N. Demon, N.A. Halim, K.W. Baharin: Methodology, Validation. All authors have read and agreed to the published version of the manuscript.

Declaration of Generative AI and AI-assisted technologies in the writing process

During the preparation of this work the author(s) used Gemini AI and Chat GPT in order to improve language and readability. After using this tool/service, the author(s) reviewed and edited the content as needed and take(s) full responsibility for the content of the publication.

Declaration of Competing Interest

The authors declare that they have no known competing financial interests or personal relationships that could have appeared to influence the work reported in this paper

Acknowledgements

Financial support from Department of Higher Education (JPT), Ministry of Higher Education Malaysia and The Science and Technology Facilities Council, United Kingdom (STFC) under Newton fund's Program and Malaysia Partnership and Alliances in Research (MyPAiR) for

research grant ISIS-NEWTON/2019/SG/01 are gratefully acknowledged. The authors also would like to acknowledge Department for Research and Innovation, UPNM for their endless support.

References

[1] H. Mali, et al., Organophosphate pesticides an emerging environmental contaminant: pollution, toxicity, bioremediation progress, and remaining challenges, J. Environ. Sci. vol. 127 (2022) 234–250, https://doi.org/10.1016/j.jes.2022.04.023.

[2] G. Bhandari, K. Atreya, P.T.J. Scheepers, V. Geissen, Concentration and distribution of pesticide residues in soil: non-dietary human health risk assessment, Chemosphere vol. 253 (2020) 126594, https://doi.org/10.1016/j.chemosphere.2020.126594.

[3] S.R. Geed, A.N. Sawarkar, R.S. Singh, B.N. Rai, New approach for biodegradation of Malathion pesticide by Bacillus sp. isolated from agricultural field: bioreactor and kinetics, J. Environ. Chem. Eng. vol. 10 (3) (2022) 107936, https://doi.org/10.1016/j.jece.2022.107936.

[4] A. Kumaravel, M. Murugananthan, R. Mangalam, S. Jayakumar, A novel, biocompatible and electrocatalytic stearic acid/nanosilver modified glassy carbon electrode for the sensing of paraoxon pesticide in food samples and commercial formulations (no. April), Food Chem. vol. 323 (2020) 126814, https://doi.org/10.1016/j.foodchem.2020.126814.

[5] Y. Liang, et al., A novel molecularly imprinted polymer composite based on polyaniline nanoparticles as sensitive sensors for parathion detection in the field (no. PB), Food Control vol. 133 (2022) 108638, https://doi.org/10.1016/j.foodcont.2021.108638.

[6] K. Barrett, F.M. Jaward, A review of endosulfan, dichlorvos, diazinon, and diuron - Pesticides used in Jamaica, Int J. Environ. Health Res vol. 22 (6) (2012) 481–499, https://doi.org/10.1080/09603123.2012.667794.

[7] V. Aroniadou-Anderjaska, J.P. Apland, T.H. Figueiredo, M. De Araujo Furtado, M. F. Braga, Acetylcholinesterase inhibitors (nerve agents) as weapons of mass destruction: history, mechanisms of action, and medical countermeasures, Neuropharmacology vol. 181 (2020) 108298, https://doi.org/10.1016/j.neuropharm.2020.108298.

[8] P.R. Giyanwani, U. Zubair, O. Salam, Z. Zubair, Respiratory failure following organophosphate poisoning: a literature review, Cureus vol. 9 (9) (2017) 3–9, https://doi.org/10.7759/cureus.1651.

[9] A. Molina, et al., A highly sensitive and biodegradable NO2 sensor made with CNTs and Ni(OH)2/NiO:Yb microparticles, J. Alloy. Compd. vol. 903 (2) (2022) 163896, https://doi.org/10.1016/j.jallcom.2022.163896.

[10] X. Lu, L. Tao, D. Song, Y. Li, F. Gao, Bimetallic Pd@Au nanorods based ultrasensitive acetylcholinesterase biosensor for determination of organophosphate pesticides, Sens Actuators B Chem. vol. 255 (2018) 2575–2581, https://doi.org/10.1016/j.snb.2017.09.063.

[11] M.M. Rahman, In-situ preparation of cadmium sulphide nanostructure decorated CNT composite materials for the development of selective benzaldehyde chemical sensor probe to remove the water contaminant by electrochemical method for environmental remediation (no. February), Mater. Chem. Phys. vol. 245 (2020) 122788, https://doi.org/10.1016/j.matchemphys.2020.122788.

[12] D. Bola, J. Alvarez-paguay, L. Fern, G. Gonz, Evaluation of an electrochemical biosensor based on carbon nanotubes, hydroxyapatite and horseradish peroxidase for the detection of hydrogen peroxide (no. August), Sens. Bio-Sens. Res. vol. 37 (2022), https://doi.org/10.1016/j.sbsr.2022.100514.

[13] J. Prakash, P.T. Rao, S. Ghorui, J. Bahadur, V. Jain, K. Dasgupta, Tailoring surface properties with O/N doping in CNT aerogel film to obtain sensitive and selective sensor for volatile organic compounds detection (no. February), Sens Actuators B Chem. vol. 359 (2022) 131606, https://doi.org/10.1016/j.snb.2022.131606.

[14] K. Nishimura, T. Ushiyama, N.X. Viet, M. Inaba, S. Kishimoto, Y. Ohno, Enhancement of the electron transfer rate in carbon nanotube flexible electrochemical sensors by surface functionalization, Electro Acta vol. 295 (2019) 157–163, https://doi.org/10.1016/j.electacta.2018.10.147.

[15] N.S.N. Sa'aya, S.Z.N. Demon, N. Abdullah, V.F.K.E.A. Shatar, N.A. Halim, Optical and morphological studies of multiwalled carbon nanotube-incorporated Poly(3-hexylthiophene-2,5-diyl) nanocomposites, Sens. Mater. vol. 31 (9) (2019) 2997–3006, https://doi.org/10.18494/SAM.2019.2513.

[16] F.G. Pacheco, A.A.C. Cotta, H.F. Gorgulho, A.P. Santos, W.A.A. Macedo, C. A. Furtado, Comparative temporal analysis of multiwalled carbon nanotube oxidation reactions: evaluating chemical modifications on true nanotube surface, Appl. Surf. Sci. vol. 357 (2015) 1015–1023, https://doi.org/10.1016/j.apsusc.2015.09.054.

[17] L.Y. Jun, N.M. Mubarak, L.S. Yon, C.H. Bing, M. Khalid, E.C. Abdullah, Comparative study of acid functionization of carbon nanotube via ultrasonic and reflux mechanism, J. Environ. Chem. Eng. vol. 6 (5) (2018) 5889–5896, https://doi.org/10.1016/j.jece.2018.09.008.

[18] N. Mohamad Saidi, N.A. Mohd Kasim, M.J. Osman, N. Janudin, I.S. Mohamad, N. Abdullah, The influences of chemical and mechanical treatment on the morphology of carbon nanofibers, Solid State Phenom. 264 (2017) 107–111, https://doi.org/10.4028/www.scientific.net/SSP.264.107.

[19] Y.G. Kim, et al., Trifluoromethyl ketone P3HT-CNT composites for chemiresistive amine sensors with improved sensitivity (no. May), Sens Actuators B Chem. vol. 367 (2022) 132076, https://doi.org/10.1016/j.snb.2022.132076.

[20] S. Chalawadi, M.S. Pujar, R.F. Bhajantri, Synthesis of CuO/polyaniline/multiwalled carbon nanotube composites using Macaranga indica leaves extract as hydrogen gas sensor, Biointerphases vol. 19 (1) (2024), https://doi.org/10.1116/6.0003282.

[21] M. Zwawi, A. Attar, A.F. Al-Hossainy, M.H. Abdel-Aziz, M.S. Zoromba, Polypyrrole/functionalized multi-walled carbon nanotube composite for optoelectronic device application, Chem. Pap. vol. 75 (12) (2021) 6575–6589, https://doi.org/10.1007/s11696-021-01830-5.

[22] S. Ebrahim, R. El-Raey, A. Hefnawy, H. Ibrahim, M. Soliman, T.M. Abdel-Fattah, Electrochemical sensor based on polyaniline nanofibers/single wall carbon nanotubes composite for detection of malathion, Synth. Met vol. 190 (Apr. 2014) 13–19, https://doi.org/10.1016/j.synthmet.2014.01.021.

[23] L. He, et al., Novel electrochemical biosensor based on core-shell nanostructured composite of hollow carbon spheres and polyaniline for sensitively detecting malathion, Sens Actuators B Chem. vol. 258 (2018) 813–821, https://doi.org/10.1016/j.snb.2017.11.161.

[24] N. Kaur, H. Thakur, N. Prabhakar, Multi walled carbon nanotubes embedded conducting polymer based electrochemical aptasensor for estimation of malathion, Microchem. J. vol. 147 (Jun. 2019) 393–402, https://doi.org/10.1016/j.microc.2019.03.042.

[25] M. Namasivayam, M.R. Andersson, J. Shapter, Role of molecularweight in polymer wrapping and dispersion of MWNT in a PVDF matrix, Polymers vol. 11 (1) (2019), https://doi.org/10.3390/polym11010162.

[26] S. Zhao, S. Hou, H. Fan, Z. Wang, J. Yu, High performance nitrogen dioxide sensor based on organic thin-film transistor utilizing P3HT/OH-MWCNTs blend film (no. June), Synth. Met 269 (2020) 116569, https://doi.org/10.1016/j.synthmet.2020.116569.

[27] T.K. Gupta, B.P. Singh, R.B. Mathur, S.R. Dhakate, Multi-walled carbon nanotube-graphene-polyaniline multiphase nanocomposite with superior electromagnetic shielding effectiveness, Nanoscale 6 (2) (2014) 842–851, https://doi.org/10.1039/c3nr04565j.

[28] H.S. Alzahrani, A.I. Al-Sulami, Q.A. Alsulami, A. Rajeh, A systematic study of structural, conductivity, linear, and nonlinear optical properties of PEO/PVA-MWCNTs/ZnO nanocomposites films for optoelectronic applications, Opt. Mater. vol. 133 (Nov. 2022) 112900, https://doi.org/10.1016/J.OPTMAT.2022.112900.

[29] T. Zhao, et al., An in-situ surface modification route for realizing the synergetic effect in P3HT-SnO2composite sensor and strikingly improving its sensing performance, Sens Actuators B Chem. vol. 241 (2) (2017) 1210–1217, https://doi.org/10.1016/j.snb.2016.10.011.

[30] X. Chen, X. Chen, X. Ding, X. Yu, X. Yu, Enhanced ammonia sensitive properties and mechanism research of PANI modified with hydroxylated single-walled nanotubes, Mater. Chem. Phys. 226 (2019) 378–386, https://doi.org/10.1016/J.MATCHEMPHYS.2019.01.061.

[31] M. Hatamzadeh, M. Jaymand, B. Massoumi, Graft copolymerization of thiophene onto polystyrene synthesized via nitroxide-mediated polymerization and its polymer – clay nanocomposite (doi:), Polym. Int 63 (3) (2014) 402–412, https://doi.org/10.1002/pi.4513.

[32] A.M. Münzer, K. Melzer, M. Heimgreiter, G. Scarpa, Random CNT network and regioregular poly(3-hexylthiophen) FETs for pH sensing applications: a comparison, Biochim Biophys. Acta Gen. Subj. 1830 (9) (2013) 4353–4358, https://doi.org/10.1016/j.bbagen.2013.01.023.

[33] P.C. Mahakul, K. Sa, B.V.R.S. Subramanyam, K.C. Patra, P. Mahanandia, Investigation of optical and electrical properties of MWCNT/rGO/poly(3-hexylthiophene) ternary composites, J. Mater. Sci. 53 (11) (2018) 8151–8160, https://doi.org/10.1007/s10853-018-2161-3.

[34] Y.G. Kim, et al., Trifluoromethyl ketone P3HT-CNT composites for chemiresistive amine sensors with improved sensitivity, Sens Actuators B Chem. 367 (2022), https://doi.org/10.1016/j.snb.2022.132076.

[35] Z. Meng, et al., A Novel Poly(3-hexylthiophene) engineered interface for electrochemical monitoring of ascorbic acid during the occurrence of glutamate-induced brain cytotoxic edemas, Research vol. 6 (2023), https://doi.org/10.34133/research.0149.

[36] A. Bartošová, L. Blinová, M. Sirotiak, A. Michalíková, Usage of FTIR-ATR as non-destructive analysis of selected toxic dyes (doi), Res. Pap. Fac. Mater. Sci. Technol. Slovak Univ. Technol. 25 (40) (2017) 103–111, https://doi.org/10.1515/rput-2017-0012.

[37] T.F. Harrelson, et al., Direct probe of the nuclear modes limiting charge mobility in molecular semiconductors, Mater. Horiz. 6 (1) (2019) 182–191, https://doi.org/10.1039/C8MH01069B.

[38] A.A.Y. Guilbert, et al., Mapping microstructural dynamics up to the nanosecond of the conjugated polymer P3HT in the solid state, Chem. Mater. 31 (23) (2019), https://doi.org/10.1021/acs.chemmater.9b02904.

[39] A.R. Rennie, A. Engberg, O. Eriksson, R.M. Dalgliesh, Understanding neutron absorption and scattering in a polymer composite material, Nucl. Instrum. Methods Phys. Res A 984 (2020), https://doi.org/10.1016/j.nima.2020.164613.

[40] W. Langel, Introduction to neutron scattering, ChemTexts vol. 9 (4) (2023), https://doi.org/10.1007/s40828-023-00184-7.

[41] P.C.H. Mitchell, S.F. Parker, A.J. Ramirez-Cuesta, J. Tomkinson, Vibrational Spectroscopy with Neutrons, vol. Volume 3, WORLD SCIENTIFIC, 2005, https://doi.org/10.1142/5628.

[42] N.M. Nurazzi, N. Abdullah, S.Z.N. Demon, N.A. Halim, I.S. Mohamad, The influence of reaction time on non-covalent functionalisation of p3ht/mwcnt nanocomposites, Polymers 13 (12) (2021), https://doi.org/10.3390/polym13121916.

[43] M. Nurazzi, N. Orcid, and N. Abdullah, "Effect of reaction time on the structure and optical properties of P3HT / MWCNT-OH nanocomposites," no. 5, pp. 0–1, 2022.

[44] L. Brambilla, et al., Infrared and multi-wavelength Raman spectroscopy of regio-regular P3HT and its deutero derivatives, J. Raman Spectrosc. 49 (3) (2018) 569–580, https://doi.org/10.1002/jrs.5301.
[45] X. Li, et al., Improved thermoelectric performance of P3HT/SWCNTs composite films by HClO4 post-treatment (no. February), Compos. Commun. 12 (2019) 128–132, https://doi.org/10.1016/j.coco.2019.01.009.
[46] Y. Piao, et al., Comparative study of multiwall carbon nanotube nanocomposites by Raman, SEM, and XPS measurement techniques (no. March), Compos Sci. Technol. 208 (2021), https://doi.org/10.1016/j.compscitech.2021.108753.
[47] M.S. Dresselhaus, A. Jorio, R. Saito, Characterizing graphene, graphite, and carbon nanotubes by Raman spectroscopy, Annu Rev. Condens Matter Phys. 1 (2010) 89–108, https://doi.org/10.1146/annurev-conmatphys-070909-103919.
[48] P.C. Eklund, J.M. Holden, R.A. Jishi, Vibrational modes of carbon nanotubes; spectroscopy and theory, Carbon N. Y 33 (7) (1995), https://doi.org/10.1016/0008-6223(95)00035-C.
[49] D. Meng, et al., Grafting P3HT brushes on GO sheets: distinctive properties of the GO/P3HT composites due to different grafting approaches, J. Mater. Chem. 22 (40) (2012), https://doi.org/10.1039/c2jm35317b.
[50] X. Zheng, H. Chen, Z. Wei, Y. Yang, H. Lin, S. Yang, High-performance, stable and low-cost mesoscopic perovskite (CH3NH3PbI3) solar cells based on poly(3-hexylthiophene)-modified carbon nanotube cathodes, Front. Optoelectron. 9 (1) (2016), https://doi.org/10.1007/s12200-016-0566-7.
[51] M. Jasna, M. Muraleedharan Pillai, A. Abhilash, P.S. Midhun, S. Jayalekshmi, M. K. Jayaraj, Polyaniline wrapped carbon nanotube/exfoliated MoS2 nanosheet composite as a promising electrode for high power supercapacitors, Carbon Trends 7 (2022), https://doi.org/10.1016/j.cartre.2022.100154.
[52] D. Maity, M. Manoharan, R.T. Rajendra Kumar, Development of the PANI/MWCNT nanocomposite-based fluorescent sensor for selective detection of aqueous ammonia, ACS Omega 5 (15) (2020), https://doi.org/10.1021/acsomega.9b02885.
[53] L. Bokobza, J. Zhang, Raman spectroscopic characterization of multiwall carbon nanotubes and of composites, Express Polym. Lett. 6 (7) (2012) 601–608, https://doi.org/10.3144/expresspolymlett.2012.63.
[54] A. Jorio, R. Saito, Raman spectroscopy for carbon nanotube applications, J. Appl. Phys. 129 (2) (2021), https://doi.org/10.1063/5.0030809.
[55] M. Giulianini, E.R. Waclawik, J.M. Bell, M. Scarselli, P. Castrucci, M. De Crescenzi, Microscopic and spectroscopic investigation of poly(3-hexylthiophene) interaction with carbon nanotubes, Polymers 3 (3) (Sep. 2011) 1433–1446, https://doi.org/10.3390/polym3031433.
[56] K. Sa, et al., Effect of reduced graphene oxide-carbon nanotubes hybrid nanofillers in mechanical properties of polymer nanocomposites, IOP Conf. Ser. Mater. Sci. Eng. 338 (1) (2018), https://doi.org/10.1088/1757-899X/338/1/012055.
[57] B. Zhang, et al., A facile synthesis of polypyrrole/carbon nanotube composites with ultrathin, uniform and thickness-tunable polypyrrole shells, Nanoscale Res Lett. 6 (1) (2011) 1–9, https://doi.org/10.1186/1556-276X-6-431.
[58] G. Quintás, S. Garrigues, M. De La Guardia, FT-Raman spectrometry determination of Malathion in pesticide formulations, Talanta 63 (2) (2004) 345–350, https://doi.org/10.1016/j.talanta.2003.11.004.
[59] Z. Yang, J. Yu, K. Fu, F. Tang, Preparation and characterization of poly (3-hexylthiophene) / carbon nanotubes hybrid material via in-situ click chemistry, Mater. Chem. Phys. 223 (2019), https://doi.org/10.1016/j.matchemphys.2018.11.050.
[60] M.E. Ramoroka, et al., Highly electro-conductive thiophene and N-methylpyrrole functionalized hyperbranched polypropylenimine tetramine-co-poly(3-hexylthiophene-2,5-diyl) donor materials for organic solar cells, J. Sci.: Adv. Mater. Devices 8 (3) (2023), https://doi.org/10.1016/j.jsamd.2023.100614.
[61] A. Hamdast, S. Agbolaghi, M. Zeighami, Y. Beygi-Khosrowshahi, R. Sarvari, Butterfly nanostructures via regioregularly grafted multi-walled carbon nanotubes and poly(3-hexylthiophene) to improve photovoltaic characteristics, Polym. Int 68 (3) (Mar. 2019) 335–343, https://doi.org/10.1002/pi.5736.
[62] Y. Du, K.F. Cai, S.Z. Shen, P.S. Casey, Preparation and characterization of graphene nanosheets/poly(3- hexylthiophene) thermoelectric composite materials, Synth. Met 162 (23) (2012) 2102–2106, https://doi.org/10.1016/j.synthmet.2012.09.011.
[63] C.C. Ortiz Yara, O.L. Ramos Sandoval, D.A. Hurtado, Identification and quantification of malathion using image analysis algorithms in infrared spectrometry, ARPN J. Eng. Appl. Sci. 11 (13) (2016) 8194–8199.
[64] C.K. Madhusudhan, R.S.P. Kumar, M. Faisal, K. Mahendra, N. Raghavendra, V. T. Vasantha, Polypyrrole coated multiwalled carbon nanotube hybrids for corrosion inhibition, Colloid J. 84 (3) (2022), https://doi.org/10.1134/S1061933X22030097.
[65] N.S.N. Sa'aya, S.Z.N. Demon, N. Abdullah, A.F.M. Azmi, N.A. Halim, Amperometric study of P3HT/Multi-walled carbon nanotubes composite for malathion sensing, Lect. Notes Mech. Eng. (2023), https://doi.org/10.1007/978-981-19-9509-5_9.
[66] G.D. Atter, D.M. Chapman, R.E. Hester, D.A. Green, P.C.H. Mitchell, J. Tomkinson, Refined ab initio inelastic neutron scattering spectrum of thiophene, J. Chem. Soc. Faraday Trans. 93 (17) (1997) 2977–2980, https://doi.org/10.1039/A702717F.
[67] D.A. Braden, S.F. Parker, J. Tomkinson, B.S. Hudson, Inelastic neutron scattering spectra of the longitudinal acoustic modes of the normal alkanes from pentane to pentacosane, J. Chem. Phys. 111 (1) (Jun. 1999) 429–437, https://doi.org/10.1063/1.479293.